MINERALOGICAL MAGAZINE

VOLUME 60 NUMBER 403 DECEMBER 1996

Orientation contrast imaging of microstructures in rocks using forescatter detectors in the scanning electron microscope

DAVID J. PRIOR, PATRICK W. TRIMBY, URSULA D.WEBER

Department of Earth Sciences, Liverpool University, L69 3BX, UK

AND

DAVID J. DINGLEY

Department of Physics, University of Bristol, UK

Abstract

We have developed a system using 'forescatter detectors' for backscattered imaging of specimen surfaces inclined at 50–80° to the incident beam (inclined-scanning) in the SEM. These detectors comprise semiconductor chips placed below the tilted specimen. Forescatter detectors provide an orientation contrast (OC) image to complement quantitative crystallographic data from electron backscatter patterns (EBSP). Specimens were imaged using two detector geometries and these images were compared to those collected with the specimen surface normal to the incident beam (normal-scanning) using conventional backscattered electron detector geometries and also to an automated technique, orientation imaging microscopy (OIM). When normal-scanning, the component of the BSE signal relating to the mean atomic number (z) of the material is an order of magnitude greater than any OC component, making OC imaging in polyphase specimens almost impossible. Images formed in inclined-scanning, using forescatter detectors, have OC and z-contrast signals of similar magnitude, allowing OC imaging in polyphase specimens.

OC imaging is purely qualitative, and by repeatedly imaging the same area using different specimen-beam geometries, we found that a single image picks out less than 60% of the total microstructural information and as many as 6 combined images are required to give the full data set. The OIM technique is limited by the EBSP resolution (1–2°) and subsequently misses a lot of microstructural information. The use of forescatter detectors is the most practical means of imaging OC in tilted specimens, but it is also a powerful tool in its own right for imaging microstructures in polyphase specimens, an essential asset for geological work.

KEYWORDS: contrast images, scanning electron microscopy, backscattered electrons.

Introduction

SELECTED area electron channelling patterns (Coates, 1967; Joy, 1974; Joy *et al.*, 1982; Davidson, 1984; Lloyd, 1985; 1987; Schmidt and Olesen, 1989; Lloyd *et al.*, 1991; Lloyd, 1995) and electron backscatter patterns (Alam *et al.*, 1954; Venables and Harland, 1972; Dingley, 1981; 1984; Dingley and Baba-Kishi, 1990; Dingley and Randle, 1992; Randle, 1992; Day, 1993) both provide quantitative data concerning spatial variation of crystallographic orientations of minerals. In many problems relevant to geologists,

Mineralogical Magazine, December 1996, Vol. 60, pp. 859–869
© *Copyright the Mineralogical Society*

the electron channelling approach has had an advantage in that it is easy to switch between a backscattered electron (BSE) image which clearly shows the specimen microstructure as orientation contrast (OC), to a selected area electron channelling pattern (SAECP) which can be used to index the crystallographic orientation of grains located using the OC image (Lloyd, 1987; 1995; Lloyd *et al.*, 1987). Orientation Contrast is generated where there are differences in the diffraction geometry of an incident beam and the crystal lattice of the specimen (Hirsch *et al.*, 1962; Newbury *et al.*, 1973; 1974), such as between grains or sub-grains of different crystallographic orientations or different crystallographic structure (Davidson, 1984; Lloyd, 1985; 1987). OC has been a valuable tool, with and without supporting SAECP data, in the study of textures in rocks (Lloyd *et al.*, 1987; Prior *et al.*, 1990; Lloyd *et al.*, 1991; 1992; Burnley *et al.*, 1991; Lloyd and Knipe., 1992; Prior, 1992; Mainprice *et al.*, 1993). Orientation Contrast has also been referred to as electron channelling contrast (ECC: Newbury *et al.*, 1974) and electron channelling contrast imaging (ECCI: Wilkinson *et al.*, 1993).

To collect an electron backscatter pattern (EBSP), the specimen needs to be tilted so that the EBSP can be recorded directly on film, or on a phosphor screen imaged by a video camera. Typically angles of 50° to 80° are required, between the normal to the specimen surface and the incident electron beam (Dingley, 1984). With this specimen geometry, conventional imaging methods, using secondary electron or pole-piece BSE detectors, do not provide an equivalent to the OC image so that in practical terms the EBSPs have been of little use to the geologist since the EBSP data cannot be related back to observed microstructures. A backscatter detector positioned on the pole piece can be used to image a specimen tilted at a high angle but the collection geometry is far from ideal so that the resultant image is of poor quality and in practice contains no resolvable OC component. In some materials (e.g. metals, calcite) it is possible to etch or decorate the specimens to reveal aspects of the microstructure and then to use the secondary electron image of a tilted specimen to locate EBSP data. However, these techniques are not generally applicable to all minerals and do not carry as much information as an OC image. Etching is often selective (Day, 1993) and it is not clear that etching of some materials (quartz for example) reveals microstructurally significant features (Prior, 1988; M. Handy, pers. comm.).

An alternative approach is to automate EBSP collection and to reconstruct the specimen microstructure from a grid-work of EBSP data-points (Adams *et al.*, 1993; Dingley and Randle, 1992; Randle, 1992; Kunze *et al.*, 1995). This technique, named orientation imaging microscopy (OIM: Adams *et al.*, 1993), is undoubtedly powerful, but represents a significant overkill for many geological problems and at present is only developed for monominerallic aggregates. The technique is also limited by the angular resolution of EBSPs; this limitation will be highlighted later on.

In early BSE studies, specimens were tilted at a high angle to the incident electron beam and BSE detectors were located in front of or below the specimen (e.g. Oatley, 1972). Adoption of this approach provides BSE images for tilted specimens and moreover, crystallographic information is carried by the electrons which are incident upon forward mounted backscatter detectors (Day, 1993; Wilkinson *et al.*, 1993). We have explored the use of these detectors to provide an OC image to accompany the EBSP technique in the analysis of rocks. We will refer to BSE detectors mounted forward of or below the specimen as forescatter detectors to distinguish these from conventional pole-piece solid-state or scintillator BSE detectors which are sited above the specimen surface. Specimen imaging with the specimen surface normal to the incident beam will be referred to as normal-scanning. Specimen imaging with the specimen-normal tilted to high angles relative to the incident beam will be referred to as inclined-scanning.

This paper presents images collected using forescatter detectors from several contrasting geological specimens. We compare and contrast these images with more conventional SEM images of the same specimens, present a physical explanation of forescatter images and discuss the use of forescatter detectors in the microstructural analysis of geological specimens.

Methods

Blocks and thin sections were polished to 0.25 μm using diamond paste on a paper lap. To remove all surface damage, specimens were then polished using the chemical-mechanical method (Fynn and Powell, 1979) on a Multipol II machine using a polyurethane lap and SYTON fluid (see Lloyd., 1987). A Philips XL30 SEM, using operating software version 5.0, was used. Normal-scanning was carried out using a KE electronics, four-quadrant, pole-piece semiconductor BSE detector with the signal amplified through a KE electronics amplifier (type 2BS3). The edges of a specimen surface were painted with conductive carbon paint (connected to earth). For normal-scanning applications, specimens were carbon coated.

The forescatter detectors were tested with the normal to the specimen surface tilted to the incident electron beam (at 70° unless otherwise stated). Two,

mutually exclusive, forescatter detector geometries have been developed:

1. Three 1 cm × 1 cm semi-conductor chips were arranged in a coplanar formation and were attached to the inclined specimen in a position below the specimen, as shown in Fig. 1*a*. The positioning of the detectors is a compromise to allow the shortest path for the BSEs to the detectors, whilst maintaining a BSE path which is close to a simple reflection, but restricting detected electrons to those with a smaller scatter angle than the reflected rays (Fig. 1*b*). A 2 mm slit aperture, made of conducting material and connected to earth, can be inserted to limit the range of scattering angles of the electrons hitting the forescatter detectors (Fig. 1*a*). The three detectors were connected to three of the channels in the BSE signal amplifier (the same amplifier as used for the pole piece detector).

2. Two coplanar 0.5 cm × 0.5 cm semi-conductor chips were attached to the base of the imaging phosphor of the EBSP camera (Fig. 1*c*). The detectors were positioned to maintain a BSE path which is close to a simple reflection path (for a specimen inclination of 70°), but allowing only electrons which have a smaller scatter angle than the reflected rays to hit the detector (Fig. 1*b*). The two detectors were connected to two of the channels in the BSE signal amplifier. Two more semi-conductor chips were attached to the top of the imaging phosphor of the EBSP camera (Fig. 1*c*) to give a backscatter detector geometry . These were connected to the remaining channels of the BSE signal amplifier. The signal of the forescatter and backscatter detectors can be separated by selecting appropriate channels on the signal amplifier.

For inclined-scanning applications the edges of the specimen surface were painted with conductive carbon paint (connected to earth) but specimens were not normally carbon coated as this significantly reduces the EBSP quality. Images of inclined specimens were tilt corrected using the Philips operating system. For all images a variety of accelerating voltages (AccV), spot sizes (Sp) and working distances (WD) were used. Specific data are given in figure captions. On inclined specimens WD is measured to the centre of the image. Spot sizes are quoted as the numbers used by the Philips operating system. At 20 kV accelerating voltage and a WD of 20 mm these correspond approximately to beam currents of: Sp5 = 0.8 nA, Sp6 = 3.2nA, Sp7 = 13.2 nA.

Backscatter coefficients (η) were measured experimentally by measuring the specimen current (I_s) and comparing this with the current measured using a Faraday Cage (I_f) at the same beam conditions and working distance. All specimen current readings were made on carbon coated specimens. Measurements were made whilst the beam was in spot mode. A special holder was designed to enable the Faraday Cage to be mounted with a specimen at any tilt. A Faraday Cage reading

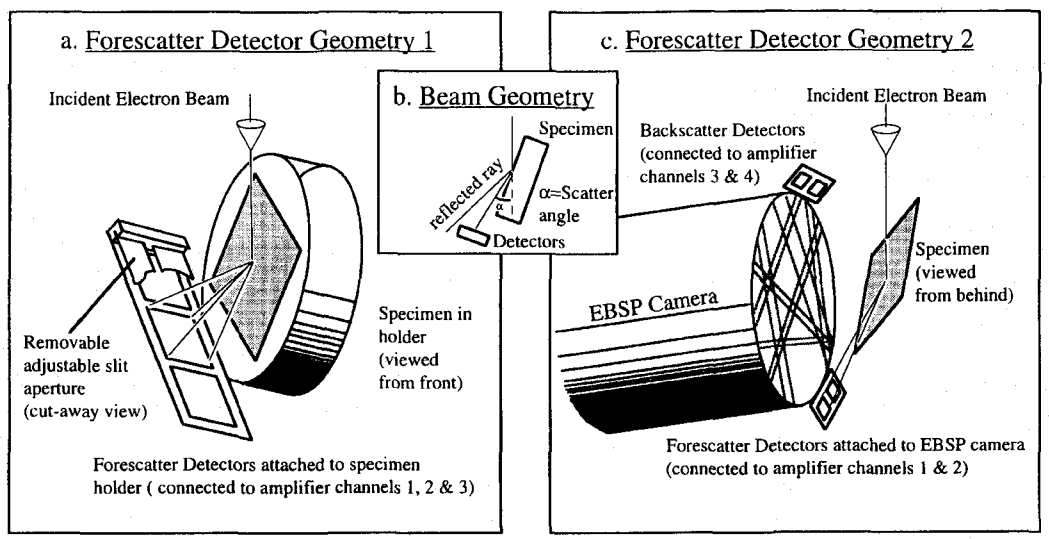

FIG. 1. Forescatter detector geometries. (*a*) Geometry 1. Three semiconductor chips attached to the specimen. Cut away shows positioning of optional apertures. (*b*) Beam-specimen-detector geometry approximated by both detector geometries. (*c*) Geometry 2. Two semiconductor chips attached to the bottom of the EBSP camera. A further two chips, attached to the top of the camera, provide a comparative BSE image.

was taken before and after each specimen reading. The backscatter coefficient approximates to the proportion of electrons leaving the specimen surface (Bishop, 1974; Loretto, 1994) and was calculated using the formula:

$$\eta = (I_f - I_s)/(I_f)$$

An OIM image was collected using facilities at TEXSEM laboratories, Provo, Utah. The image was generated from a grid of 11,000 EBSP points spaced 1 μm apart. Acquisition time was approximately 12 hours.

The response of forescatter detectors to compositional and crystallographic variations

An eclogite from the Tauern region of Austria (Fig. 2) and a granite from Peru (Fig. 3) are typical of many geological materials in that they contain many phases. Backscattered Electrons have provided an excellent way of imaging phases of different composition (Hall and Lloyd., 1981; Lloyd and Hall, 1981; Krinsley *et al.*, 1983; White *et al.*, 1984; Lloyd, 1985; 1987) and the eclogite and granite provide good examples of this (Figs 2*a*, 3*a,c*). However, normal-scanning OC images within one phase are often compromised by the presence of other phases. In normal-scanning, the most significant component of the BSE signal relates to the mean atomic number (z-contrast) of the material being imaged (Goldstein *et al.*, 1981; Lloyd, 1985) and the electron channelling effect which provides an OC image is at least an order of magnitude less significant. In order to see the OC image within any one phase the gain on the BSE amplifier has to be turned up to such a degree that the signals from

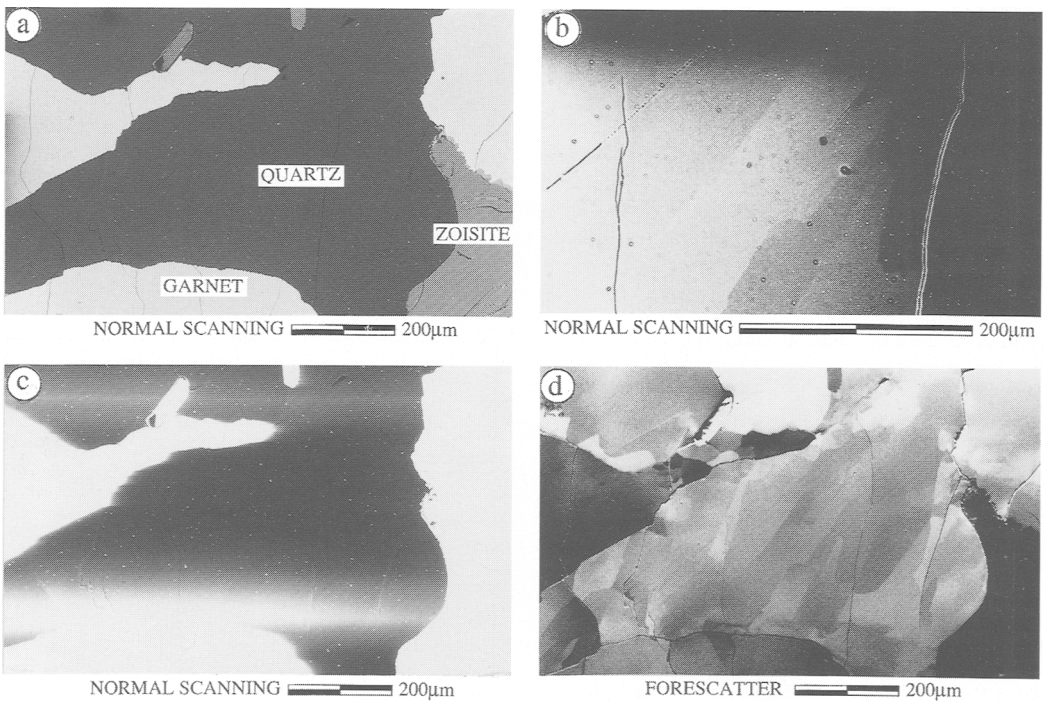

FIG. 2. SEM photomicrographs of an eclogite specimen from the Tauern area, Austria. (*a*) Normal-scanning BSE image showing clear z-contrast between garnet, zoisite and quartz. WD 26 mm, AccV 20 kV, Sp 5. (*b*) Normal-scanning BSE image taken from within the quartz in (*a*). Beam energy is high and the gain on the amplifier has been turned up to show OC within the quartz. WD 8 mm, AccV 20 kV, Sp 7. (*c*) Normal-scanning BSE image of the same area shown in (*a*), but with the same beam conditions and amplifier gain used in (*b*). All useful OC information is lost due to artifacts (most notably 'gain stripes') caused by the extreme BSE contrast between garnet and quartz. (*d*) Inclined-scanning image using forescatter detectors of the same area imaged in (*a*). Sub-grains are clearly visible in both quartz and garnet as a result of significant OC contrast. There is no significant or consistent z-contrast between the phases. WD 26 mm, AccV 20 kV, Sp 5. Forescatter geometry 1.

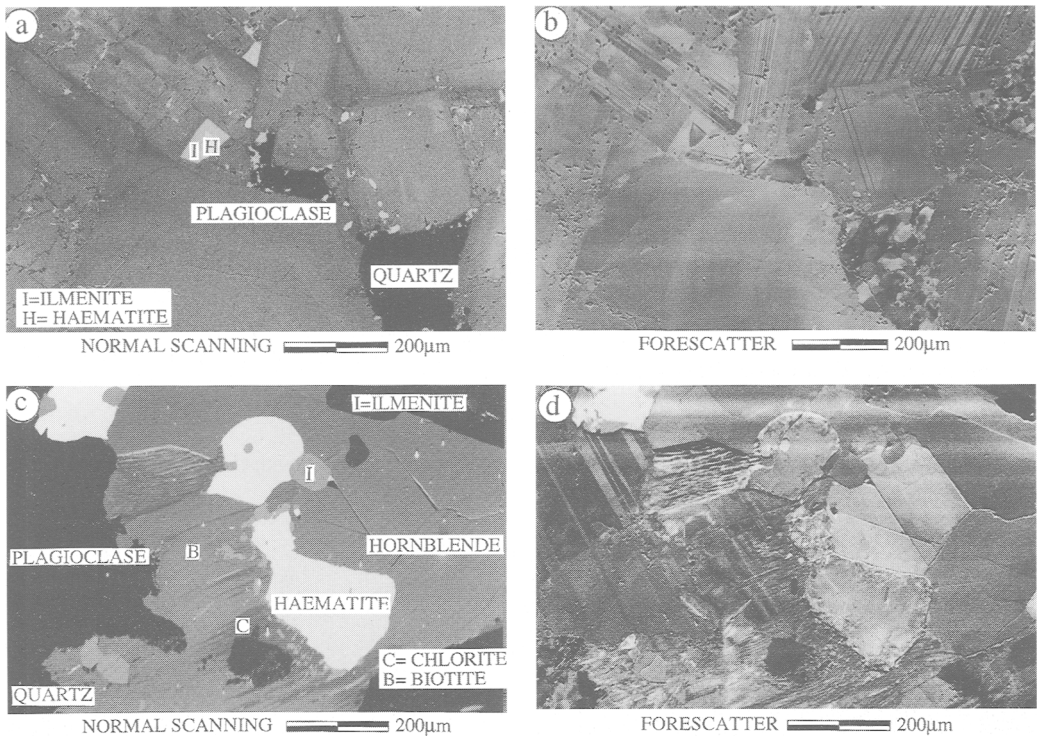

FIG. 3. SEM photomicrographs of a granite from Peru. (*a*) Normal-scanning BSE image showing clear z-contrast between plagioclase, quartz, hematite and ilmenite. The z-contrast image shows compositional zoning parallel to grain boundaries in the plagioclase. WD 20 mm, AccV 20 kV, Sp 5. (*b*) Inclined-scanning image using forescatter detectors of the same area imaged in (*a*). Sub-grains are clearly visible in quartz and twins and sub-grains are visible in plagioclase as a result of significant OC contrast. There is no significant or consistent z-contrast between the phases. WD 30 mm, AccV 20 kV, Sp 5. Forescatter geometry 1. (*c*) Inclined-scanning BSE image using pole-piece detectors showing clear z-contrast between plagioclase, quartz, biotite, chlorite, hornblende, hematite and ilmenite. WD 20 mm, AccV 20 kV, Sp 5. (*d*) Inclined-scanning image using forescatter detectors of the same area imaged in (*c*). OC is very strong and detailed substructures are visible in all phases. OC is of greater magnitude than z-contrast. WD 30 mm, AccV 20 kV, Sp 5. Forescatter geometry 1.

any second phases present are pushed beyond the white or black limits. This can cause problems: a common effect is that the signal amplifier cannot recover from these perturbations within the time period of one scan width so that the area to the right of a second phase will be masked by a 'gain stripe' (Fig. 2*b*, *c*). One interesting and very useful aspect of the inclined-scanning images collected using the forescatter detectors (Figs 2*d*, 3*b*) is that the OC and z-contrast signals are of similar magnitude. Forescatter detectors may be used for OC imaging in polyphase specimens which may be difficult or impossible to image in normal-scanning. It is possible to collect limited OC microstructural data in normal-scanning of polyphase specimens by using magnification and rotation to ensure that the image contains only one phase or that the phase of interest is entirely on the left hand side of the image (e.g. Fig. 2*b* and figures in Prior *et al.*, 1990). Some microstructures are impossible to image in normal-scanning OC images, a good example is that of the internal structure of a quartz inclusion in garnet. Using inclined-scanning OC images the quartz inclusion microstructure is easily resolved.

Experimental studies and numerical simulations (Kanter, 1957; Newbury *et al.*, 1973; Bishop, 1974) show that the backscatter coefficient (the fraction of electrons scattered out of the sample) increases as the incident beam angle shallows from normal to the specimen surface but the ratio of backscatter

coefficients of any two elements decreases. These data have been used to generate an approximate empirical relationship for pure elements (Goldstein *et al.*, 1981), between specimen inclination and backscatter coefficient (η):

$$\eta\ (\vartheta) = 1/(1 + \cos\ \vartheta)^p$$

where $p = 9/\sqrt{z}$, ϑ = angle of inclination (between beam and specimen normal) z = atomic number of the element.

This relationship is shown graphically in Fig. 4*a* for atomic numbers equivalent to the mean atomic numbers of hematite, biotite, plagioclase and quartz. BSE contrasts (δ) have been calculated from the data shown in Fig. 4*a* using the following relationship (Lloyd, 1985):

$$\delta = (\eta_A - \eta_B)/0.5(\eta_A + \eta_B)$$

where η_A and η_B are the backscatter coefficients of the two contrasting phases. Variations in BSE contrast with tilt are shown in Fig. 4*b*. Direct measurements of backscatter coefficients of hematite, biotite, plagioclase and quartz in the granite have been made at different tilt angles. These data are shown in Fig. 4*c*.

The data in Fig. 4 show that BSE coefficients increase with specimen inclination whilst z-contrast decreases. There is a reduction in z-contrast at specimen inclinations of 70° of more than 50% compared to normal-scanning images (Fig. 4*b*). The electrons which strike the forescatter detectors are high energy, elastically scattered electrons. They are not scattered through >90° as BSEs collected in normal-scanning must be. For the forescatter configurations used in this paper, electrons are scattered between 20° and 39°. Elastic scattering by individual atoms (Hirsch *et al.*, 1965) is associated with two events (Loretto, 1994); a contribution of Rutherford scattering from the nucleus and a scattering contribution from the electron cloud. At smaller scattering angles the nucleus contribution is less and it follows that the low angle scattering is less dependent upon the mean atomic number (z) of the specimen than is high angle scattering. Interactions of electrons with a lattice are more complicated, in that the electron cloud structure is modified and one must consider multiple elastic interactions (Loretto, 1994; Goldstein *et al.*, 1981), but it seems likely that a similar relationship should hold. The theoretical analyses suggest that the z-contrast should be reduced at low scatter angles, but that the total signal should be enhanced. Since the incident electrons will still be diffracted by the lattice it follows that the low scatter-angle electrons should contain a strong OC component.

An examination of micrographs illustrates that the data in Fig. 4, which relate to the total backscatter

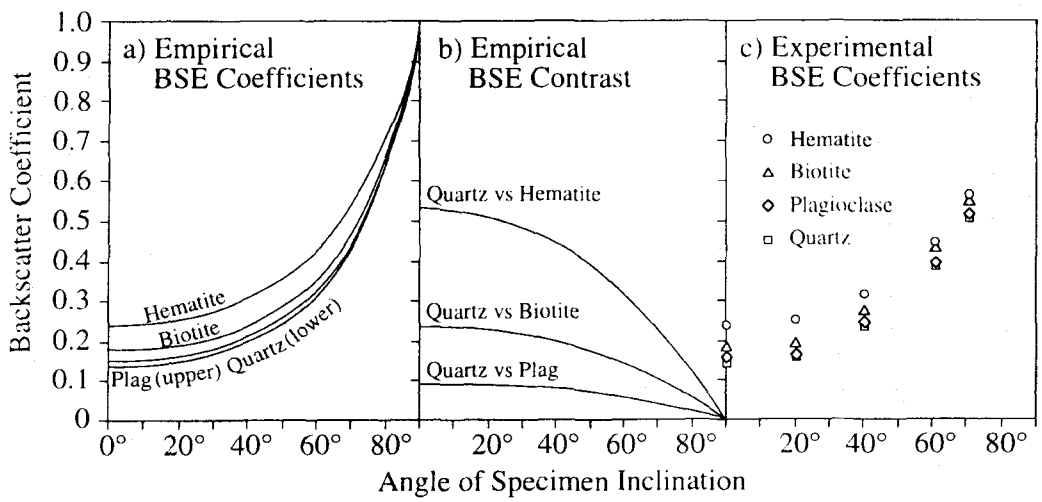

FIG. 4. (*a*) Plot of BSE coefficients against specimen inclination for elements with atomic number approximately equivalent to quartz, plagioclase, biotite and hematite. Plot is constructed from empirical relationships (Goldstein *et al.*, 1981). See text for details. (*b*) Plot showing the influence of specimen inclination on the BSE contrast between an element with approximately the same atomic number as quartz and elements with atomic numbers equivalent to plagioclase, biotite and hematite. See text for details. (*c*) Measured BSE coefficients for quartz, plagioclase, biotite and hematite at different specimen inclinations. At each inclination the specimen current was measured for 10 grains of each phase and the mean BSE coefficient plotted. See methods section for procedures and text for discussion. The specimen is the granite shown in Fig. 3.

signal, represent an oversimplification. At specimen inclinations of 70°, forescatter detectors detect an OC signal which is as strong as the z-contrast whilst the pole-piece BSE detector detects an OC signal that is much smaller than very small z-contrast signals (e.g. between quartz and plagioclase). These observations suggest that OC is enhanced or z-contrast is subdued at low scatter angles and that an analysis of BSE coefficient magnitudes that does not account for detector position is not sufficient. The total z-contrast does decrease with specimen inclination but, this is complicated by a variation from a z-contrast signal at high scatter angles to an OC signal at low scatter angles. A series of physical extensions were attached to forescatter geometry 1 to investigate experimentally the effects of increased electron scatter-angle at constant specimen inclination (70°). These extensions allow imaging BSEs that have been deflected 50 to 65°, 80 to 90° and 120 to 140° and provide a spectrum of detector response between the forescatter position (20–39°) and the pole-piece detector (160–180°). In practical terms the cut off of strong OC is sharp. Where the beam has been scattered through 60° or more, images are dominated by the z-contrast component.

Processes which potentially give OC components are electron channelling (EC) and diffraction of BSEs. Electron Channelling is conventionally used to explain OC in normal-scanning. Some incident electrons will undergo low angle scattering and diffraction and will be 'channelled' into the specimen to a depth where they are unlikely to escape following further elastic interactions. In grains of different orientation, the proportion of electrons channelled in will vary and the BSE signal will vary as a result (Newbury *et al.*, 1973, 1974). Diffraction of the BSEs leaving the specimen also gives contrast variations which relate to the specimen orientation. Day (1993) argues that in inclined specimens, using forescatter detectors, the OC signal relates to this 'channelling out' rather than 'channelling in'. The most persuasive argument for 'channelling out' is that, with the specimen-beam geometry fixed, variations in the specimen-detector geometry give rise to significant variations in an OC image. This is an effect we have been able to reproduce in inclined-scanning by separating the signals from individual detectors and in normal-scanning by separating the signals of the four quadrants of the pole-piece detector.

Sensitivity to variations in crystallographic orientation: towards a quantitative OC image

A quartz mylonite from the Lewisian near Torridon (Law *et al.*, 1990; Lloyd *et al.*, 1992; Mainprice *et al.*, 1993) provides an ideal sample to test the effectiveness of an OC type image. Much of this specimen comprises extremely fine grained quartz with no second phase. Figure 5 shows comparative images collected in normal-scanning using the pole-piece detector and inclined-scanning using the forescatter detector system. The normal-scanning image and the images from the forescatter detectors are comparable; all are OC images. There are differences in the distributions of grey shades in the three images that relate, in part at least, to the differences in incident beam and detector geometries. It has always been clear that OC images are qualitative (Joy, 1974; Lloyd, 1985; 1987). The grey level of a given grain cannot be inverted to give the crystallographic orientation and geometrical coincidences can lead to some boundaries with crystallographic mismatch being invisible. Grain grey-levels and boundary topology of normal and inclined-scanning OC images are affected by specimen working distance (WD). This effect is most noticeable at short WDs where there is maximum variation in incident beam orientation (Lloyd, 1987). Normal and inclined-scanning OC images are similarly affected by specimen orientation (rotation on an axis normal to the specimen surface) and inclined-scanning OC images are similarly affected by tilt angle.

Variations due to WD and tilt allow us to constrain more of the boundaries in both normal and inclined-scanning images. Eight inclined-scanning OC images, with different tilt angles, were collected of the same area. Two of these images are presented in Fig. 5*b-c*. No two of the images in Fig. 5, or any of the images not shown, are the same. A boundary map can be made using data from all eight forescatter images. A regular grid was placed over each image. The grid was positioned in the same relative position on each image using visible surface imperfections (scratches, etch pits etc). The grid was used to compare the number of grain boundaries in each image. For example the total number of boundaries discernible in three of the images could be compared with the total number discernible in all eight of the images. The results of this analysis are shown graphically in Fig. 6. It is worrying that any individual OC image contains an average of only 58% of the grain boundary information. Compilation of data from six images is needed to constrain all of the boundaries, although data from four images constrains over 90% of the grain boundary information.

An OIM image was collected for an area and compared to a single forescatter image (Fig. 7). The OIM image is fully quantitative and this provides a standard showing all of the changes in crystallographic orientation within the specimen, within the angular resolution of automated EBSP work. It is

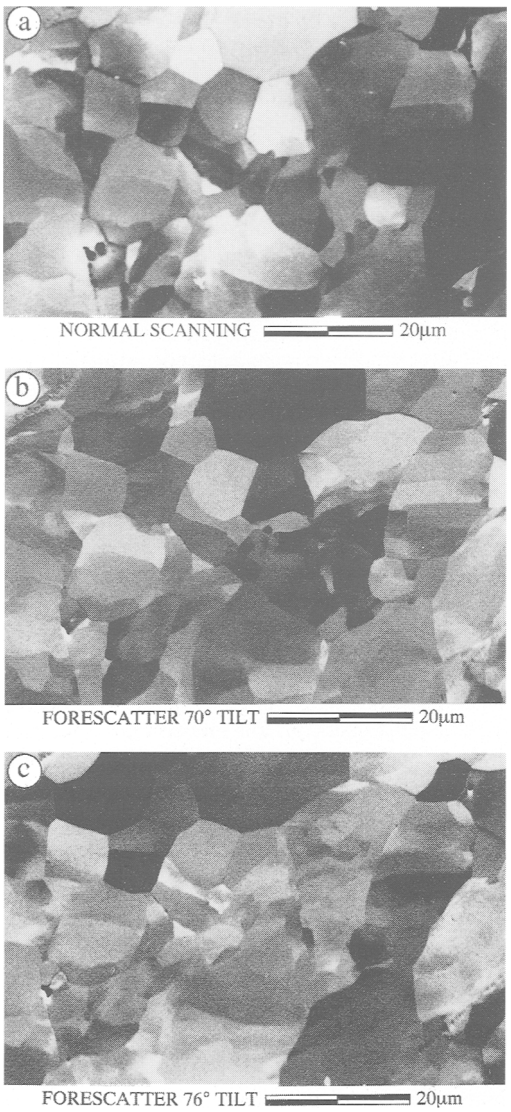

FIG. 5. SEM photomicrographs of the microstructure of a quartz mylonite from Torridon, N.W. Scotland. (*a*) Normal-scanning BSE image with a high beam energy and with the gain on the amplifier turned up to show OC within the quartz. WD 8 mm, AccV 20 kV, Sp 7. (*b*) Inclined-scanning image using forescatter detectors of the same area imaged in (*a*) with a specimen inclination of 70°. WD 26 mm, AccV 25 kV, Sp 4 Forescatter geometry 1. (*c*) As (*b*) but with a specimen inclination of 76°.

clear that the grain-size imaged on the OIM is considerably larger than that imaged by the

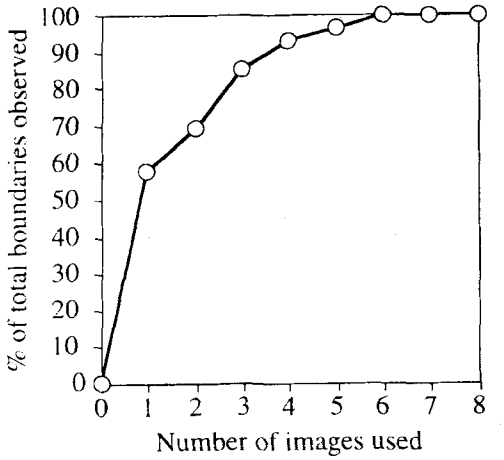

FIG. 6. Plot of the number of grain boundaries detectable by combining data from 1, 2, 3, 4, 5, 6 and 7 images expressed as a percentage of the number visible by combining the data from all eight images.

forescatter detectors and that the OIM misses as much as 50% of the available microstructural information. These boundaries, omitted by the OIM, must be boundaries below the resolution limit of angular changes for EBSP patterns. In our own experiments re-indexing of the same grain using EBSP gives an angular precision of about 1–2°, based on 100 measurements on quartz and 20 on garnet. Thus the OC images are detecting a significant number of boundaries with mismatches of less than 1–2°.

Although a complete boundary map can be generated by combining the data from different images with different geometries it would be better to develop an imaging system which highlights all the orientation mismatches in live time. Individual images from the three forescatter detectors (geometry 1) show contrasting microstructures analogous to those from different specimen tilts. Live overlay of these images does not enhance the grain boundary resolution as there may be as much destructive as constructive interference in the image and some boundaries may remain hidden. Day (1993) has had some success using a computer overlay of the three separate images, coloured using three primary colours (colour orientation contrast images: COCI). Our data suggest that successful COCI work needs rather more than three detectors. A system using eight detectors is being developed at the National Physical Laboratory (Austin Day; pers. comm.).

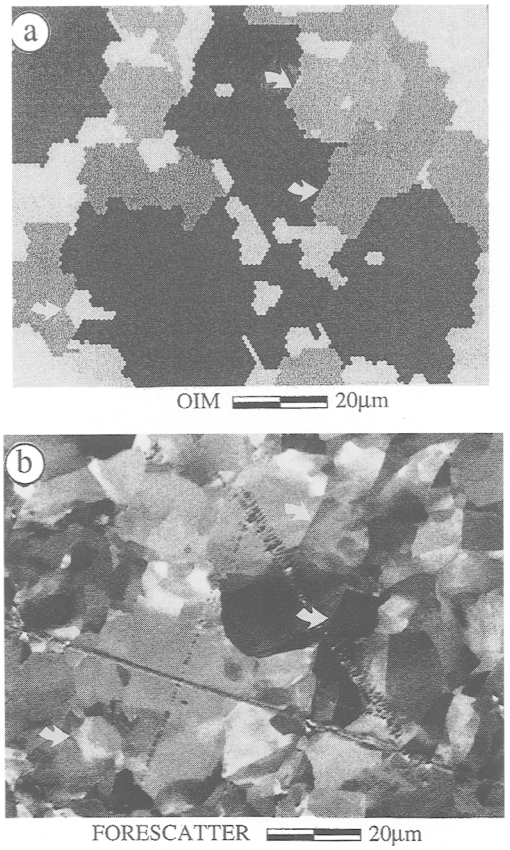

FIG. 7. (*a*) Grain map of the microstructure of a quartz mylonite from Torridon, N.W. Scotland, as constructed from Orientation Imaging Microscopy. (*b*) SEM photomicrograph of the same area using forescatter detectors in geometry 1 with a specimen inclination of 70°. The two images are slightly distorted with respect to each other. To help orient the reader, three white arrows on each image point to equivalent boundaries. WD 24 mm, AccV 25 kV, Sp 4. See text for discussion.

Practical use of forescatter detectors

The two forescatter geometries developed in this paper give comparable results. Geometry 1 gives higher quality images than geometry 2, presumably because the detectors are much closer to the specimen. The quality difference is more noticeable in polyphase specimens than in monominerallic ones. More energy is required to generate comparative images using geometry 2 as compared to geometry 1. Provided the same working distance is used, geometry 2 maintains the same angular relationships between the specimen and detector ; geometry 1 does not. It is essential to have several detectors in geometry 1 to maintain a balanced signal in images from all parts of the specimen. It is always possible to use the EBSP camera in conjunction with geometry 2. Geometry 1 forescatter detectors may cast a shadow on the EBSP camera. The size of the shadow is dependent upon which part of the specimen is being examined. Aperturing of geometry 1 gave no significant change in imaging except for an overall reduction in signal strength. The quality of the images is strongly dependent upon the quality of the signal amplifier used with the detectors. When specimens are tilted to high angles, the number of emitted electrons (BSE and SE) approaches and then exceeds the number of incident electrons (Gopinath, 1974) so that charging should not be a problem. Some specimens do adhere to this theoretical behaviour and in most specimens charging is not a problem at low magnification and beam energy. At higher magnifications and the high beam energies needed for practical EBSP work on geological minerals (and also to obtain pole-piece BSE images of highly-tilted specimens), specimen charging can be a problem. Charging problems are worse with poorly polished or dirty/dusty specimens. The effects of charging are that meaningful SE images are not obtainable (especially at high magnifications), BSE images undergo continuous shift and temporary and permanent specimen surface damage can occur. Carbon coated specimens can be imaged but the quality of the OC image and of EBSP patterns is severely reduced unless the carbon coat is extremely thin.

With a specimen inclination of 70° surface contamination of any sort can severely degrade image quality as the contaminant particles throw long shadows and contribute to charge build up. It is particularly important that specimen surfaces are kept dust free.

Orientation Contrast on inclined specimens using forescatter detectors is so strong that it is difficult to tell phases apart. Thus use of the forescatter detector image alone on polyphase specimens can be problematic and in practice it is necessary to use another image to distinguish phases. One possibility is to pre-montage the specimen using normal-scanning. This remains the method which will give the best quality z-contrast image but may be inappropriate for reconnaissance type investigations. For inclined-scanning the specimen is best uncoated and this precludes switching from inclined to normal scanning in one session. A practical alternative is to use the pole piece BSE detector, or the quadrants located above the EBSP camera in detector geometry 2, whilst the specimen is tilted. Neither of these give a z contrast image to compete with the normal-scanning BSE image, but either or both may be serviceable for the purposes of phase identification

and can be used at the same time as the forescatter detectors without adjusting the specimen or beam geometry. Secondary electron images can be used but are more prone to charging problems. High magnification SE images are not generally possible. Provided the X-ray detector is positioned appropriately, qualitative X-ray analyses are possible on inclined specimens.

In practice, OC images are possible at much lower beam energies in inclined-scanning and can give better spatial resolution than normal-scanning OC images. Lower beam energies mean that the specimen activation volume is smaller (Goldstein *et al.*, 1981). However, the geometry of the activation volume is distorted when the incident beam is not normal to the specimen surface (Murata, 1973; 1974; Goldstein *et al.*, 1981). Inclined-scanning images will have lower resolution than normal-scanning images of the same beam energy. Furthermore, the spatial resolution of inclined-scanning images will be anisotropic (with lower resolution perpendicular to the tilt axis) and the majority of the BSEs which form the image will exit the specimen surface from below the point struck by the incident beam (Goldstein *et al.*, 1981). This effect must be considered when interpreting inclined-scanning images and most particularly when interpreting EBSP or X-Ray data from spot analyses.

Scanning Electron Microscopy tilt correction procedures do not always provide perfect restoration of the image to match normal scanned images. Standard tilt corrections can only correct for rotations around the scan direction. If the specimen is not flat, the tilt correction will introduce distortions. Specimen holders which ensure flat specimen surfaces are important if tilt correction is to be used. Even if the specimen is flat, the beam-specimen geometry is highly variable across the scanned area of an inclined specimen, especially at low magnifications, and in practice restoration is not perfect. If precise image restoration is important, as it is for analysis of shapes, and orientations, then comparative normal-scanning images and computer based image manipulation packages are needed.

Conclusions

Forescatter detectors provide the most practical means of imaging OC in tilted specimens and are therefore essential if EBSP data are to be collected within multi-grained monominerallic domains.

Inclined-scanning images using forescatter detectors are an important microstructural analysis tool in their own right. They provide the only practical means of collecting OC images in many multi-phase specimens since the z-contrast is of the same order of magnitude as the orientation contrast.

Orientation contrast images resolve microstructural variation well below the resolution limits of quantitative crystallographic studies using EBSPs.

Acknowledgements

Kees Veltkamp is thanked for maintaining the SEM equipment and providing assistance and advice. John Hakes advised in hard-wiring the forescatter detectors. Mark Jahme built the specimen holders and other hardware and Jim Forbes prepared some of the specimens. Dave Bryon loaned us the granite specimen. Semi-conductor chips were provided by K.E. Electronics and we are particularly grateful to Mike Cowham for his advice in their use and for the loan of equipment. Damian Dingley is thanked for his considerable assistance in providing the OIM data and updating the Liverpool EBSP software. We are grateful to Geoff Lloyd for discussions concerning the theory and practical application of forescatter detectors and particularly to Austin Day for sending a copy of his excellent PhD thesis and details of the NPL forescatter system. The Liverpool SEM was funded through the Research Task Force of the University of Liverpool. P. Trimby and U. Weber are in receipt of grants from NERC and DAAD respectively.

References

Adams, B.L., Wright, S.I. and Kunze, K. (1993) *Metall. Trans.*, **24A**, 819–30.

Alam, M.N., Blackman, M. and Pashley, D.W. (1954) *Proc. Roy. Soc.*, **222**, 224–42.

Bishop, H.E. (1974) In *Quantitative Scanning Electron Microscopy* (D.B. Holt, M.D. Muir, I.M. Boswarva and P.R. Grant, eds). Academic Press, New York.

Burnley, P., Green, H.W. II. and Prior, D.J. (1991) *J. Geophys. Res.* **96**, 425–43.

Coates, D.G. (1967) *Philos. Mag.* **16**, 1179–84.

Davidson, D.L. (1984) *Int. Metal. Rev.* **29**, 75–95.

Day, A. (1993) PhD thesis, University of Bristol.

Dingley D.J. and Randle, V. (1992) *J. Mater. Sci.* **27**, 4545–66.

Dingley, D.J. (1981) *Scanning Electron Microscopy*, **1981-IV**, 273–86.

Dingley, D.J. (1984) *Scanning Electron Microscopy*, **1984-II**, 569–75.

Dingley, D.J. and Baba-Kishi (1990) *Microscopy and Analysis*, May, 35–7.

Fynn , G.W. and Powell, W.J.A. (1979) *The Cutting and Polishing of Electro-optic Materials.* Adams Hilger, London.

Goldstein, J.I., Newbury, D.E., Echlin, P., Joy, D.C., Fiori, C. and Lifshin, E. (1981) *Scanning Electron Microscopy and X-Ray Analysis.* Plenum Press.

Gopinath. (1974) In *Quantitative Scanning Electron*

Microscopy (D.B. Holt, M.D. Muir, I.M. Boswarva and P.R. Grant, eds). Academic Press, New York.

Hall, M.G. and Lloyd, G.E. (1981) *Amer. Mineral.*, **66**, 362–8.

Hirsch , P.B., Howie, A. and Whelan, M.J. (1962) *Philos. Mag.* **7**, 2095–100.

Hirsch , P.B., Howie, A., Nicholson, R.B., Pashley, D.W. and Whelan, M.J. (1965) *Electron Microscopy of Thin Crystals.* Butterworths. London.

Joy , D.C., Newbury, D.E. and Davidson, D.L. (1982) *J. Appl. Phys.*, **55**, R81–R22.

Joy, D.C. (1974) In *Quantitative Scanning Electron Microscopy* (D.B. Holt, M.D. Muir, I.M. Boswarva and P.R. Grant, eds). Academic Press, New York.

Kanter, H. (1957) *Ann. Phys.*, **20**, 144–66.

Krinsley, D.H., Pye, K. and Kearsley, A.T. (1983) *Geol. Mag.*, **120**, 109–14.

Kunze, K., Heidelbach, F., Wenke, H-R. and Adams, B.L. (1995) In *Textures of Geological Materials* (H.J. Bunge, S. Siegesmunde, W. Skrotski and K. Weber, eds) DGM Informationsgesellschaft MbH.

Law, R.D., Schmid, S.M. and Wheeler, J. (1990) *J. Struct. Geol.*, **12**, 29–45.

Lloyd, G.E. (1985) In *Applications of Electron Microscopy in the Earth Sciences* (J.C. White ed.) *Mineral. Assoc. Can. Short Course*, **11**, 151–88.

Lloyd, G.E. and Hall, M.G. (1981) *Tectonophysics*, **78**, 687–98.

Lloyd, G.E. and Knipe, R.J. (1992) *J. Struct. Geol.*, **14**, 127–43.

Lloyd, G.E. (1987) *Mineral. Mag.*, **51**, 3–19.

Lloyd, G.E. (1995) In *Textures of Geological Materials* (H.J. Bunge, S. Siegesmunde, W. Skrotski and K. Weber, eds) DGM Informationsgesellschaft MbH.

Lloyd, G.E., Ferguson, C.C. and Law, R.D., (1987) *Tectonophysics*, **135**, 243–9.

Lloyd, G.E., Law, R.D., Mainprice, D. and Wheeler, J. (1992) *J. Struct. Geol.*, **14**, 1079–100.

Lloyd, G.E., Schmidt, N.H., Mainprice, D. and Prior, D.J. (1991) *Mineral. Mag.*, **55**, 331–45.

Loretto, M.H. (1994) *Electron Beam Analysis of Materials.* Chapman and Hall, London.

Mainprice, D., Lloyd, G.E. and Casey, M. (1993) *J. Struct. Geol.*, **15**, 1169–87.

Murata, K. (1973) SEM / 1973 IIT Research Institute, Chicago, Illinois, 268.

Murata, K. (1974) *J. Appl. Phys.*, **45**, 4110.

Newbury D.E. and Yakowitz H. (1976) *National Bureau of Standards Spec. Pub.*, **460** (K.F.J. Heinrich, D.E. Newbury and H. Yakowitz, eds) Washington, DC, 15.

Newbury, D.E., Yakowitz, H. and Yew, N. (1974) *Appl. Phys. Lett.*, **24**, 98.

Newbury, D.E., Joy, D.C., Echlin, P., Fiori, C.E. and Goldstein, J.I. (1973) *Advanced Scanning Electron Microscopy and X-Ray Microanalysis.* Plenum Press, New York.

Oatley, C.W. (1972) *The Scanning Electron Microscope.* Cambridge University Press.

Prior, D.J (1988) PhD thesis, University of Leeds.

Prior, D.J. (1993) *Contrib. Mineral. Petrol.*, **113**, 545–56.

Prior, D.J., Knipe, R.J. and Handy, M.R. (1990) In *Deformation Mechanisms, Rheology and Tectonics* (R.J. Knipe and E.H. Rutter, eds) Spec. Publ. Geol. Soc. Lond., **54**, 309–20.

Randle, V. (1992) *Microtexture Determination and its Applications.* The Institute of Materials. London.

Schmidt, N.H. and Olesen, N.Ø. (1989) *Canad. Mineral.*, **27**, 15–22.

Venables, J.A. and Harland, C.J. (1972) *Philos. Mag.*, **27**, 1193–200.

Wells, O.C. (1974) *Scanning Electron Microscopy.* McGraw Hill, New York.

White, S.H., Shaw, H.F. and Huggett, J.M. (1984) *J. Sed. Petr.*, **54**, 487–94.

Wilkinson, A.J., Anstis, G.R., Czernuska, J.T., Long, N.J. and Hirsch, P.B. (1993) *Philos. Mag. A. Phys. Cond. Matt. Defects and Mechanical Properties*, **68**, 59–80.

[*Manuscript received 20 December 1995: revised 10 April 1996*]